Geosci. Model Dev., 10, 1–18, 2017
www.geosci-model-dev.net/10/1/2017/
doi:10.5194/gmd-10-1-2017

Geoscientific Model Development
Open Access
EGU

Improving the inter-hemispheric gradient of total column atmospheric CO_2 and CH_4 in simulations with the ECMWF semi-Lagrangian atmospheric global model

Anna Agusti-Panareda[1], Michail Diamantakis[1], Victor Bayona[1], Friedrich Klappenbach[2], and Andre Butz[2]

[1]European Centre for Medium-Range Weather Forecasts, Reading, UK
[2]IMK-ASF, Karlsruhe Institute of Technology (KIT), Leopoldshafen, Germany

Correspondence to: Anna Agusti-Panareda (anna.agusti-panareda@ecmwf.int)

Received: 2 June 2016 – Published in Geosci. Model Dev. Discuss.: 14 July 2016
Revised: 28 October 2016 – Accepted: 21 November 2016 – Published: 2 January 2017

Abstract. It is a widely established fact that standard semi-Lagrangian advection schemes are highly efficient numerical techniques for simulating the transport of atmospheric tracers. However, as they are not formally mass conserving, it is essential to use some method for restoring mass conservation in long time range forecasts. A common approach is to use global mass fixers. This is the case of the semi-Lagrangian advection scheme in the Integrated Forecasting System (IFS) model used by the Copernicus Atmosphere Monitoring Service (CAMS) at the European Centre for Medium-Range Weather Forecasts (ECMWF).

Mass fixers are algorithms with substantial differences in complexity and sophistication but in general of low computational cost. This paper shows the positive impact mass fixers have on the inter-hemispheric gradient of total atmospheric column-averaged CO_2 and CH_4, a crucial feature of their spatial distribution. Two algorithms are compared: the simple "proportional" and the more complex Bermejo–Conde schemes. The former is widely used by several Earth system climate models as well the CAMS global forecasts and analysis of atmospheric composition, while the latter has been recently implemented in IFS. Comparisons against total column observations demonstrate that the proportional mass fixer is shown to be suitable for the low-resolution simulations, but for the high-resolution simulations the Bermejo–Conde scheme clearly gives better results. These results have potential repercussions for climate Earth system models using proportional mass fixers as their resolution increases. It also emphasises the importance of benchmarking the tracer mass fixers with the inter-hemispheric gradient of long-lived greenhouse gases using observations.

1 Introduction

The monitoring and prediction of climate change relies on accurately modelling the long-lived greenhouse gases using Earth system models (ESMs) (e.g. Jones et al., 2013; Keppel-Aleks et al., 2013). Carbon dioxide (CO_2) and methane (CH_4) are the most important anthropogenic greenhouse gases (Forster et al., 2007). Because of their relevance to climate mitigation and policy making, they are monitored using flux inversion systems based on atmospheric chemical transport models (CTMs) (e.g. Gurney et al., 2002; Kirschke et al., 2013). Complementing the climate monitoring, global analyses and forecasts of CO_2 and CH_4 are also performed each day as part of the Copernicus Atmosphere Monitoring Service (CAMS) (Agustí-Panareda et al., 2014; Massart et al., 2014) at the European Centre for Medium-Range Weather Forecasts (ECMWF) using the Integrated Forecasting System (IFS, www.ecmwf.int/en/forecasts/documentation-and-support/changes-ecmwf-model/ifs-documentation).

Both atmospheric CO_2 and CH_4 are characterised by a trend associated with an annual growth rate, a seasonal cycle and an inter-hemispheric gradient, which is consistent with the temporal and spatial distribution of their sources and sinks, tropopause height and atmospheric transport (Keppel-Aleks et al., 2011; Saito et al., 2012). In ESMs and CTMs the

transport is modelled using advection, convection and turbulent mixing schemes based on numerical weather prediction (NWP) methods. The semi-Lagrangian (SL) advection scheme is widely used in NWP (e.g. the ECMWF IFS model, Environment Canada GEM model; de Grandpré et al., 2016) and ESMs (e.g. ACCESS, HadGM2; documented by Corbin and Law, 2011; Collins et al., 2011) because of its high numerical stability, accuracy and computational efficiency. Furthermore, for the problem of multiple tracer advection, it is undeniably the most efficient approach given that for each tracer the transport operation reduces to interpolating the field from the fixed grid to the time-step-dependent departure point grid. The latter is re-computed only once at each new time step, which implies that the same interpolation weights can be used for all tracers (and prognostic fields in general). However, the non-flux form of the SL scheme by default does not conserve mass. This can lead to small errors in the global mass of tracers when modelling the tracer advection. In the case of CH_4 and CO_2, these errors accumulate with time because there is a slow or non-existent chemical sink in the atmosphere. It is therefore imperative to apply a mass fixer in order to restore the conservation of the total tracer mass. This is particularly important for CO_2, as the mass conservation error can reach values that are as large as the observed global mass trend resulting from their surface fluxes and can significantly distort its large-scale distribution (e.g. Houweling et al., 2010). There are several methods to fix the global tracer mass, from the simple proportional mass fixers to more sophisticated algorithms that focus the correction where the conservation error associated with the tracer advection is assumed to be largest, i.e. in the regions with strongest gradients. Because of its simplicity, the proportional mass fixer is widely used by ESMs and NWP models (Collins et al., 2011; Corbin and Law, 2011; Agustí-Panareda et al., 2014; Flemming et al., 2015). There are different implementations of the global proportional mass fixer. However, the correction procedure is very homogeneous/uniform. For this reason, it is prone to the artificial transfer of mass and long-range propagation of errors (Jöckel et al., 2001). Therefore, it has the potential to create a distortion in the inter-hemispheric gradient of tracers (Maksyutov et al., 2008).

Diamantakis and Flemming (2014) implemented and tested several of these global mass fixers on the humidity, cloud fields and ozone in the IFS. Both CO_2 and CH_4 have different characteristics and requirements than shorter-lived reactive gases and humidity. Because of their long life, they are generally well-mixed with smooth gradients, and large background values relative to their gradients. Their large-scale spatial variability is characterised by a relatively weak inter-hemispheric gradient (of the order of 100 ppb or 5 % for CH_4 and 10 ppm or 2.5 % for CO_2). Nevertheless, it constitutes a crucial feature to represent in the models because it reflects the spatial distribution of the surface sources and/or sinks (Dargaville et al., 2003; Patra et al., 2011). Considering these properties and the computational cost, flexibility and efficiency, the Bermejo and Conde (2002) fixer is deemed to be the most suited among the available schemes in the IFS for the modelling requirements of the long-lived greenhouse gases. This is consistent with the recent tests performed with the Environment Canada Semi-Lagrangian Model by de Grandpré et al. (2016) and Polavarapu et al. (2016).

This paper presents a comparison of a customised Bermejo and Conde (2002) mass fixer and the proportional mass fixer, which was operational until recently in the CAMS CO_2 and CH_4 forecasting and analysis system (Agustí-Panareda et al., 2014; Massart et al., 2014), and it is also widely used in Earth system climate models (Corbin and Law, 2011; Collins et al., 2011; Jones et al., 2011). The impact of the two mass fixers on the preservation of the CO_2 and CH_4 inter-hemispheric gradient is a crucial benchmark for testing their suitability in any CO_2 and CH_4 forecasting and analysis system. Furthermore, this study can provide valuable feedback to the Earth system climate models using the simple global proportional mass fixer. The impact of resolution on the mass conservation and performance of the mass fixers can help guide the choice of mass fixer in future climate simulations.

The structure the paper is as follows: in Sect. 2 the mass fixers are described; the experiments performed to test the impact of the mass fixers are presented in Sect. 3; the observations are documented in Sect. 4; the results from the experiments and their evaluation using observations are provided in Sect. 5; a summary of the main findings is given in Sect. 6.

2 Global tracer mass fixers

The two tracer mass fixers selected in this study are described in this section. The algorithms of these fixers are described in detail by Diamantakis and Flemming (2014) as part of a set available in the ECMWF IFS model. Thus, their notation is used henceforth. A few minor modifications have been necessary in order to fine-tune these algorithms for simulating the transport of long-lived greenhouse gases. For example, it was found that, given that a mass mixing ratio formulation is used, a small mass conservation error in the total atmospheric mass after advection can lead to a systematic accumulation of the tracer mass conservation error with time. This stems from the fact that the global mass of a tracer is computed using surface pressure (see Eq. 1 below), that the mass conservation error always has the same sign, and finally that there are no atmospheric processes (e.g. strong chemical sources and/or sinks) that can counter the effect of the systematic error accumulation. It was therefore necessary to apply the mass fixer on surface pressure as well, as explained in the paragraphs below.

The IFS is a hydrostatic model using a pressure-based coordinate system which implies that the surface pressure field is required to compute the total tracer mass. For example, the mass of a tracer χ with mass mixing ratio $\phi_\chi = \rho_\chi / \rho$, where

ρ_χ, ρ the tracer and air-density respectively, is given by

$$M(\phi_\chi, p) = \sum_{j=1}^{N} A_j \sum_{k=1}^{K} \phi_{jk} \frac{\Delta p_{jk}}{g}, \quad (1)$$

where p is the atmospheric pressure field, A_j is the horizontal surface area of box j, k is the vertical model level and g the gravitational constant. Each model level consists of N grid points and there are K vertical levels.

Experiments with IFS at different resolutions showed that it is important that after the advection step and before the mass of the tracer is corrected, the pressure field needs to be corrected in order to ensure that the total mass of air

$$M(p) = \sum_{j=1}^{N} A_j \sum_{k=1}^{K} \frac{\Delta p_{jk}}{g} \quad (2)$$

is globally conserved in the tracer mass computation. We did not find large differences in the method of correction applied here, and this can be done either by the proportional algorithm (described below) or by the McGregor scheme described also in Diamantakis and Flemming (2014). The latter was chosen as it gives realistic corrections of surface pressure in regions with cyclonic activity or regions with orography and additionally has very low computational cost. For a model using a height-based vertical coordinate system and density as the prognostic variable, the correction should be applied on density. In the following sections, the pressure after the SL advection is always corrected to have the same global value as before advection by using the proportional fixer presented below.

2.1 Global proportional mass fixer

The proportional mass fixer only requires the computation of the total tracer mass before and after the SL advection step. The mixing ratio of every single grid point is then multiplied by the same scaling factor, i.e.

$$\left(\phi_\chi\right)_{jk} = \alpha\left(\phi^*_\chi\right)_{jk}, \quad \alpha = \frac{M(\phi^0_\chi, p^0)}{M(\phi^*_\chi, p^*)},$$

where (ϕ^0_χ, p^0) and (ϕ^*_χ, p^*) are the tracer mixing ratio and the pressure field before and after the SL advection step respectively. Long-lived tracers also require the correction of the pressure field to ensure global mass conservation of air before computing the scaling factor α, as already discussed at the beginning of Sect. 2. The advantages of this fixer is that it is computationally cheap, it is easy to implement, it preserves positive definiteness, and for tracers such as CO_2 and CH_4 it produces very small increments. The disadvantage is that the mass of every grid point is adjusted by the same factor implying that regions with large transport and mass conservation error are corrected by an equal proportion with regions where these errors are small; therefore, the solution deteriorates there. This scheme is used by the ACCESS (Corbin and Law, 2011) and HadGEM-2 (Collins et al., 2011; Jones et al., 2011) Earth system climate models.

2.2 Bermejo–Conde mass fixer

A 3-D version of the Bermejo and Conde (2002) mass fixer has been implemented in the IFS (Diamantakis and Flemming, 2014) that provides an effective alternative to the proportional global mass fixer for the simulation of long-lived greenhouse gases. This scheme preserves the monotonicity of an advected field (provided the original field is also monotone) and overall the increments it computes are small. A weighted approach is used where a different weighting factor is applied when correcting the mass mixing ratios of different grid points. For grid points in regions where the field is smooth the weights are very small and the correction is negligible. However, for grid points in regions with large gradients the weight and therefore the computed increments are larger. This is the major advantage of this method, which is well suited for simulating the transport of long-lived gases such as CO_2 and CH_4. These species are spread everywhere on the globe, being fairly uniform in some geographical regions (e.g. Antarctica), while they have considerable gradients in other regions (e.g. Africa, South America). Furthermore, the mass conserving field the scheme computes has minimum distance from the original advected non-conserving field as it is the solution to a minimisation problem which ensures that the increments are overall small.

Using the notation of the previous section and ignoring for simplicity the subscript χ, the correction the Bermejo–Conde scheme introduces to the grid-point mixing ratio in IFS can be written as

$$\phi_{jk} = \phi^*_{jk} - \lambda w_{jk}, \quad \lambda = \frac{\delta M}{\sum_{j=1}^{N} A_j \sum_{k=1}^{K} w_{jk} \frac{\Delta p^*_{jk}}{g}}, \quad (3)$$

where $\delta M = M(\phi^*_\chi, p^*) - M(\phi^0_\chi, p^0)$ is the small global mass error. In this case, we have chosen

$$w_{jk} = \max\left[0, \operatorname{sgn}(\delta M)\operatorname{sgn}\left(\phi^*_{jk} - \phi^{\mathrm{L}}_{jk}\right)\left|\phi^*_{jk} - \phi^{\mathrm{L}}_{jk}\right|^{\beta} \frac{p_{jk}}{p_{j0}}\right], \quad (4)$$

which depends on the difference between the cubic interpolated field ϕ^* and the linear one ϕ^{L} as described in Diamantakis and Flemming (2014). It was argued there that an appropriate setting for the parameter β would be 1. This conclusion was based on testing done with moist and fast chemically active tracers which differ considerably from long-lived tracers. Repeating these tests on CO_2 and CH_4, we found that using $\beta = 2$ is working more effectively. That is, the weights w_{jk} become even smaller in smooth regions and larger in regions with mass gradients. As this is an even number, $\operatorname{sgn}\left(\phi^*_{jk} - \phi^L_{jk}\right)$ needs to be considered in Eq. (4) to allow preservation of monotonicity and positive definiteness. Moreover, to avoid erroneously large corrections in the

Table 1. List of simulations at different resolutions and with different mass fixers performed from 1 March 2013 to 30 April 2014.

Experiment description	Model grid resolution	Advection time step (s)
High resolution without fixer	TL1279, L137	600
High resolution with proportional fixer	TL1279, L137	600
High resolution with Bermejo–Conde fixer	TL1279, L137	600
Low resolution without fixer	TL255, L60	2700
Low resolution with proportional fixer	TL255, L60	2700
Low resolution with Bermejo–Conde fixer	TL255, L60	2700

Table 2. List of the TCCON stations used in this study and ordered by latitude from north to south.

Site	Lat	Long	Reference
Eureka	80.05	−86.42	Strong et al. (2014)
Sodankylä	67.37	26.63	Kivi et al. (2014)
Karlsruhe	49.10	8.44	Hase et al. (2014)
Garmisch	47.48	11.06	Sussmann and Rettinger (2014)
Park Falls	45.94	−90.27	Wennberg et al. (2014a)
Rikubetsu	43.46	−143.77	Morino et al. (2014)
Lamont	36.60	−97.49	Wennberg et al. (2014b)
Izaña	28.30	−16.48	Blumenstock et al. (2014)
Ascension Island	−7.92	−14.33	Feist et al. (2014)
Darwin	−12.43	130.89	Griffith et al. (2014a)
Wollongong	−34.41	150.88	Griffith et al. (2014b)
Lauder 125HR	−45.05	169.68	Sherlock et al. (2014)

stratosphere, the weight w_{jk} is scaled by a factor of $\frac{p_{jk}}{p_{j0}}$ that reflects the density variation from the surface to the top of the atmosphere. Since IFS uses a pressure-based vertical coordinate, a good option is the ratio of the pressure at grid point jk (p_{jk}) to the surface pressure below this grid point (p_{j0}).

3 Experiments

Several CO_2 and CH_4 simulations using the IFS have been performed to test the influence of the global tracer mass fixers on their inter-hemispheric gradient. The global proportional fixer has been used for the low-resolution simulations and shown to provide satisfactory results in terms of gradients in the CO_2 simulation (Agustí-Panareda et al., 2014) and CH_4 in the Transcom model intercomparison studies (Saito et al., 2013; Locatelli et al., 2013). However, it is not clear whether this is still the case for the high-resolution simulations. For this reason, the global proportional fixer is compared with the Bermejo and Conde (2002) fixer using two different resolutions. One is a low resolution corresponding to approximately 80 km in the horizontal with 60 model levels, i.e. the same as the one used by the ECMWF ERA-Interim reanalysis and similar to that used in climate simulations (e.g. Collins et al., 2011). The other resolution is approximately 16 km in the horizontal and 137 model levels, i.e. following the operational NWP resolution also used in the operational CO_2 and CH_4 CAMS forecasts. The model time steps depend on the model resolution, corresponding to 10 and 45 min for high and low resolutions respectively. A list of all the experiments can be found in Table 1.

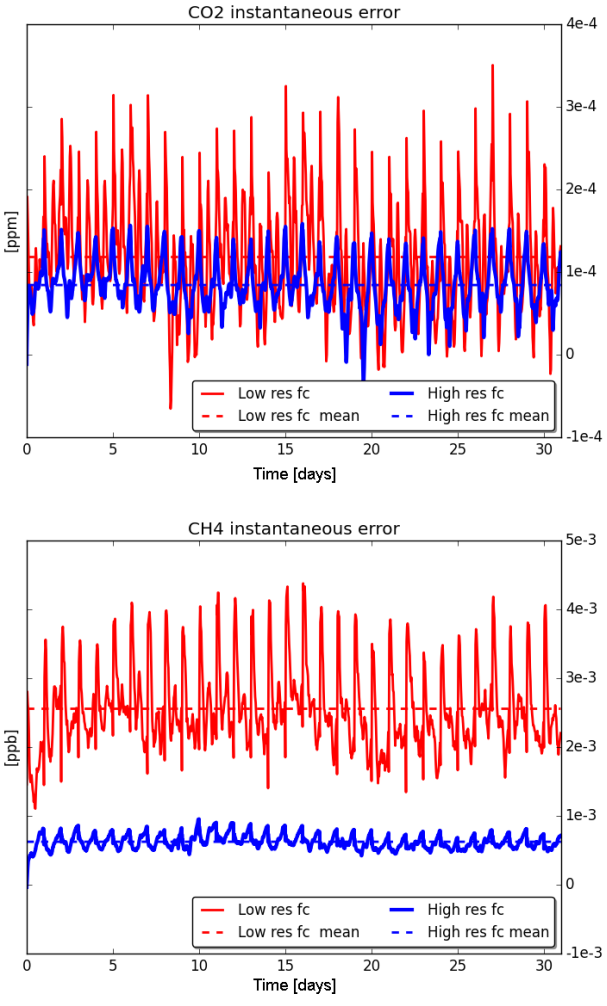

Figure 1. Instantaneous global mean mass conservation error for CO_2 (ppm) and CH_4 (ppb) from 1 to 31 March 2013. Low- and high-resolution experiments are depicted by red and blue lines respectively.

The simulations are performed using the cyclic forecast configuration with the IFS NWP model. This means that the meteorology is re-initialised at 00:00 UTC using the operational ECMWF NWP analysis, but the CO_2 and CH_4 tracers are allowed to evolve freely, i.e. without any constraint from observations. The transport in the IFS is based on the semi-Lagrangian advection scheme (Temperton et al., 2001; Hortal, 2002; Untch and Hortal, 2006) described in the previous section, as well as a turbulent mixing scheme (Beljaars and Viterbo, 1998; Koehler et al., 2011; Sandu et al., 2013) and a convection scheme (Tiedtke, 1989; Bechtold et al., 2008, 2014).

The CH_4 fluxes and chemical sink in the simulations are based on prescribed climatologies and inventories as used by the operational CAMS CH_4 analysis and forecast (see Massart et al., 2014) following the prior fluxes and chemical sink of Bergamaschi et al. (2009) flux inversion system, except for the fire emissions from the GFAS dataset (Kaiser et al., 2012). The surface fluxes of CO_2 are also the same as those used in the operational CO_2 analysis and forecast (see Agustí-Panareda et al., 2014, for a detailed description). They are all prescribed from inventories and climatologies, except for the land biogenic CO_2 fluxes which are modelled online by the CTESSEL Carbon module (Boussetta et al., 2013). A flux adjustment scheme has been implemented to correct for biases in the NEE budget with respect to a climatology of optimised fluxes from Chevallier et al. (2010) (see Agustí-Panareda et al., 2016, for further details). The fluxes for the high and low resolution are based on the same inventories and model. The global budget for the prescribed fluxes is the same, but their resolution is different. Because of that the gradients are sharper in the high resolution as the emission hotspots are characterised by stronger fluxes with the same mass distributed over a smaller area. For the modelled fluxes, the climate drivers such as radiation, soil moisture and temperature might vary with the resolution, and therefore the fluxes will not necessarily be the same. This only affects CO_2 as CH_4 only has prescribed fluxes.

The CO_2 and CH_4 simulations have been performed from 1 March 2013 to 30 April 2014. The aim is to test the annual accumulation of the error associated with mass conservation and the impact of the implemented mass fixer. In order to focus on the accumulated impact, instead of the mean impact, the evaluation of the simulations is done for the last month, and not the whole period. The last month from 7 March to 10 April was used to compare with the observations from the *Polarstern* cruise (Klappenbach et al., 2015) providing a north–south transect across the Atlantic of total column-averaged CO_2 and CH_4, together with observations from the Total Carbon Column Observing Network (TCCON) (Wunch et al., 2011). A description of the observations used to assess the experiments is given in the next section.

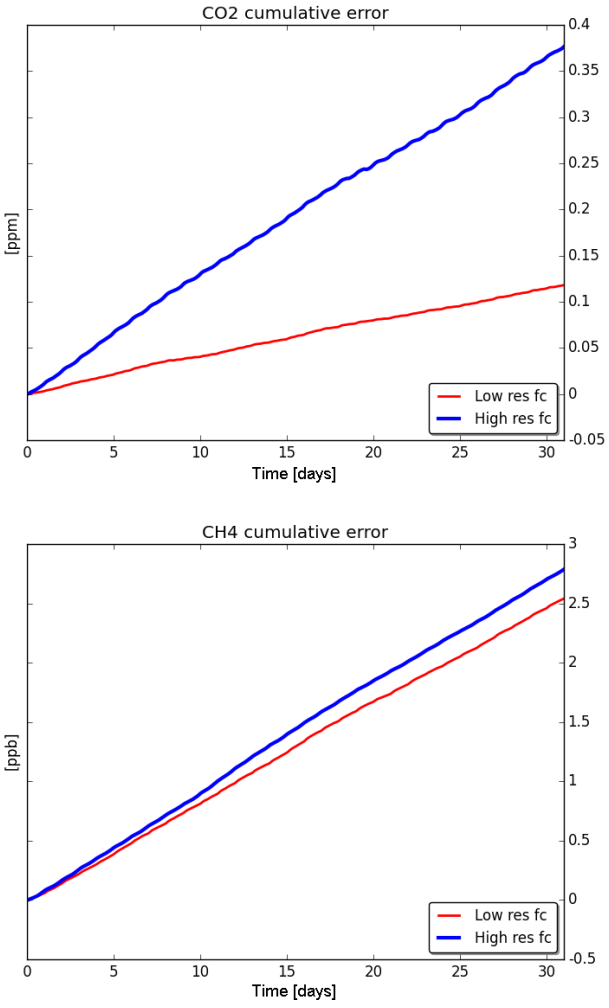

Figure 2. Cumulative global mean mass conservation error for CO_2 (ppm) and CH_4 (ppb) from 1 to 31 March 2013. Low- and high-resolution experiments are depicted by red and blue lines respectively.

4 Observations

The ship-based *Polarstern* dataset (Klappenbach et al., 2015) provides an excellent opportunity to assess the inter-hemispheric gradient, as it samples mainly oceanic well-mixed background air. The research vessel *Polarstern* took off from Cape Town (34° S, 18° E), South Africa, on 5 March 2014, and entered port at Bremerhaven (54° N, 19° E), Germany, on 14 April 2014. During the cruise, an EM27/SUN near-infrared spectrometer was deployed onboard *Polarstern*. It collected direct-sun absorption spectra allowing the retrieval of XCO_2 and XCH_4 with high precision and accuracy (Gisi et al., 2012; Hase et al., 2015; Frey et al., 2015) as detailed for the *Polarstern* campaign by Klappenbach et al. (2015). Post-campaign deployment of the EM27/SUN side by side the TCCON spectrometer at Karlsruhe, Germany, allowed the calibration of XCO_2 and

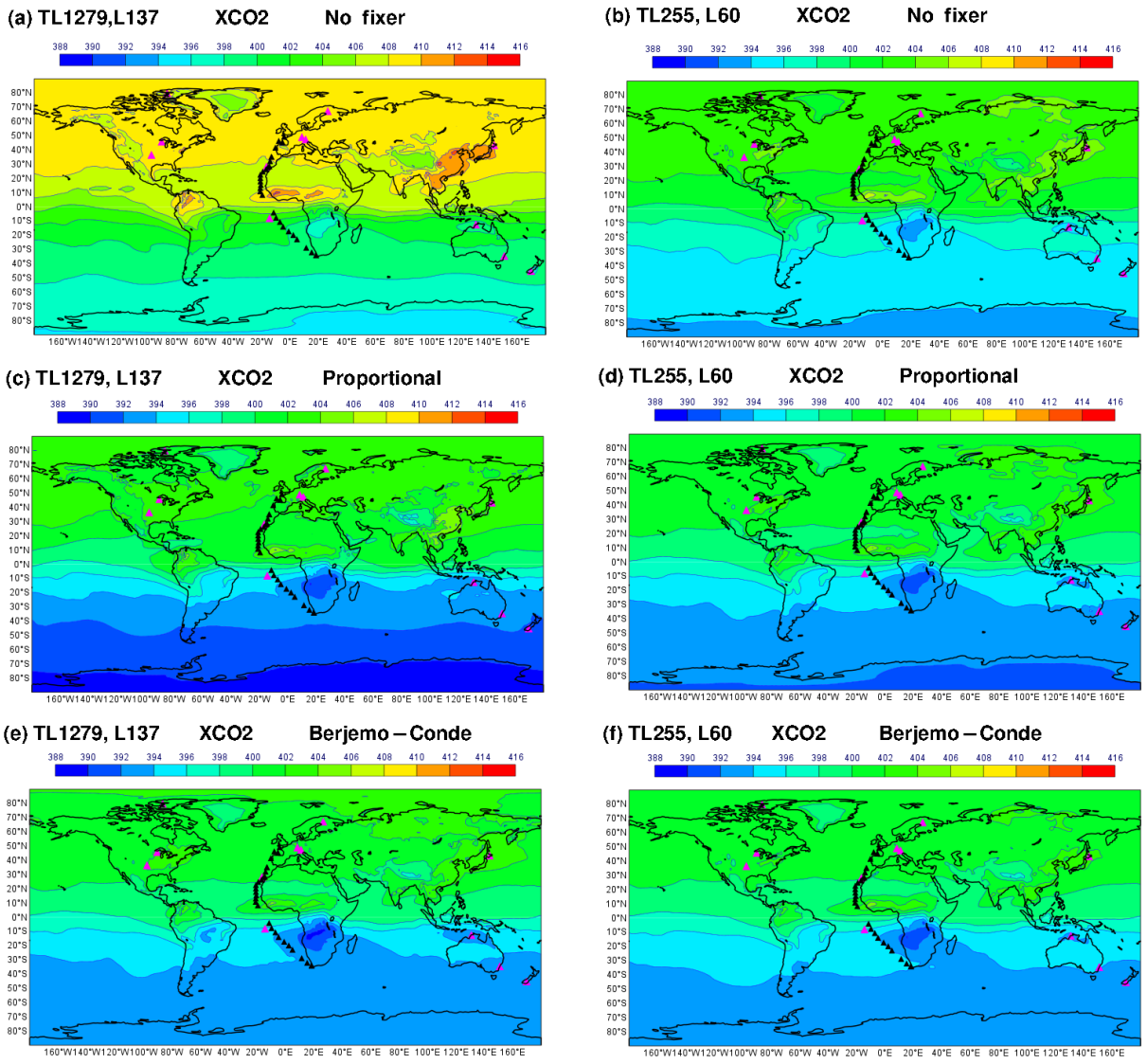

Figure 3. Mean XCO_2 (ppm) from 7 March to 10 April 2014 for the high-resolution (left panels) and low-resolution (right panels) simulations. The effect of the different mass fixers is shown in the different rows. Details of the simulations can be found in Table 1. The pink and black triangles mark the location of the reference observations from TCCON and *Polarstern* cruise respectively. See Table 2 for a list of the TCCON site coordinates.

XCH_4 to the World Meteorological Organization (WMO) standard. Klappenbach et al. (2015) estimated the precision of the retrieved mole fractions to be to better than 0.2 ppm and 0.7 ppb for XCO_2 and XCH_4, respectively. This remote sensing technique samples the entire total column abundance and it is less dependent on localised sources in comparison to in situ measurements.

All observations from 40° S to 40° N across the eastern Atlantic Ocean were used. Information on the prior and averaging kernel was also used in order to be able to compare the observations with the model following Rodgers and Connor (2003).

While *Polarstern* data provide a clear sampling of the meridional profile of background air representative of the large-scale inter-hemispheric gradient, they are not part of an operational network. For this reason, the evaluation of the inter-hemispheric gradient is corroborated using the TCCON observations. Observations from the TCCON (Wunch et al., 2011) are regularly used as a reference of total column CO_2 and CH_4 to calibrate and evaluate CO_2 and CH_4 products by the satellite community (e.g. Butz et al., 2011; Oshchepkov et al., 2013) and modelling community (Keppel-Aleks et al., 2011; Saito et al., 2012; Agustí-Panareda et al., 2014; Massart et al., 2016, e.g.). In this study, we used the version GGG2014 of the TCCON data (Wunch et al.,

2015, tccon.ornl.gov). TCCON sites used to assess the inter-hemispheric gradient are listed in Table 2.

5 Results

The impact of the mass fixers is assessed with global budget diagnostics (Sect. 5.1), monthly mean total column maps (Sect. 5.2) and comparisons with observations of the inter-hemispheric gradient (Sect. 5.3).

For the global mass diagnostics, the mass of the CO_2 and CH_4 tracers is computed using Eq. (1). In the results that follow, the global error in tracer mass conservation during the advection to be corrected is computed as molar fraction in part per million following

$$DM = \frac{M(\phi^*, p^*) - M(\phi^o, p^o)}{M(p^o)} \frac{m_{\text{air}}}{m_{\text{CO}_2}} \times 10^6, \quad (5)$$

where p^* is the pressure field after advection, which has been corrected with a mass fixer to conserve global atmospheric mass (i.e. $M(p^o) = M(p^*)$).

5.1 Global mass conservation error

The instantaneous global mean mass conservation error per time step computed for the low- and high-resolution simulations using Eq. (5) is mostly positive (Fig. 1). The value oscillates around 1.2×10^{-4} ppm for CO_2 and around 2.6×10^{-3} ppb for CH_4 in the low-resolution simulation. The error in the high-resolution simulation is only slightly lower for CO_2 (0.8×10^{-4} ppm) and much lower for CH_4 (0.6×10^{-3} ppb) than in the low-resolution simulation. The oscillations around the mean value are also smaller.

Although the instantaneous global mass conservation error per time step is small relative to the mean value of CO_2 and CH_4 (400 ppm and 1800 ppb respectively), the error is accumulated during the simulation. If the simulation is not re-initialised but cycled from one day to the next as in cyclic forecasts Agustí-Panareda et al. (2014) or climate runs, then this error will grow with time as shown in Fig. 2. The error growth rate is faster in the high resolution than in the low-resolution simulation by a factor of 3.2 for CO_2 and 1.1 for CH_4, despite the smaller instantaneous errors in the high-resolution simulation. This is because the time step is a factor of 4.5 smaller than in the low-resolution simulation. Therefore, the advection scheme is called more frequently, leading to a faster error accumulation. After 1 month, the conservation error reaches the value of 0.37 ppm for CO_2 and 2.79 ppb for CH_4 in the high-resolution simulation. This is equivalent to an annual growth of 4.4 ppm year^{-1} and 33.0 ppb year^{-1} for CO_2 and CH_4 respectively. These error values are larger than the current observed growth of CO_2 (from 1 to 3 ppm year^{-1}; see Le Quéré et al., 2014) and CH_4 (from 0.6 to 16 ppb year^{-1}; see Dlugokencky et al., 2009; Kirschke et al., 2013).

5.2 Impact of mass fixers on total column CO_2 and CH_4 spatial distribution

The maps of mean XCO_2 and XCH_4 from 7 March to 10 April 2014 during the period of the *Polarstern* cruise (Figs. 3 and 4) highlight the dominant inter-hemispheric gradient. After approximately 1 year of simulation without the mass fixer, the mean values of XCO_2 and XCH_4 are much higher everywhere, but particularly in the source regions in the Northern Hemisphere (e.g. over Southeast Asia). The high-resolution simulation in Figs. 4a and 3a displays an enhanced increase with respect to the low-resolution simulation (Figs. 3b and 4b). For example, in Southeast Asia the XCO_2 enhancement is around 4 ppm and the XCH_4 enhancement is around 40 ppb.

Both proportional and Bermejo–Conde mass fixers reduce the mean XCO_2 and XCH_4 values everywhere, as intended. However, the proportional mass fixer leads to slightly different spatial distribution for the high- and low-resolution simulations (Figs. 3c, d and 4c, d), whereas the two spatial distributions obtained by using Bermejo–Conde remain closer to one another for the two different resolutions (Figs. 3e, f and 4e, f). Some differences in the regions of sources and sinks are expected since the surface fluxes are also affected by the resolution change. For example, emission hotspots can be distributed over a smaller area and become more intense. However, this is not the case over Antarctica and the Southern Ocean, where surface fluxes are very weak. The impact of the resolution south of 40° S is indeed striking, particularly for the proportional mass fixer (Figs. 3c, d and 4c, d). Over that region the mean XCO_2 and XCH_4 are 2 to 4 ppm and 20 to 40 ppb lower in the proportional mass fixer simulation at high resolution than all other simulations. This large-scale mean negative difference cannot be explained by differences in fluxes or transport. Thus, it has to be linked to the mass conservation error and the effect of the proportional mass fixer, enhanced by the action of the mass fixer at high resolution (see Sect. 5.1).

The effect of the mass fixers can be seen more clearly in Figs. 5 and 6 by computing the difference between the fields resulting from the different mass fixers with the fields from the simulation without any mass fixer. The proportional mass fixer removes mass quite uniformly for both the high- and low-resolution simulations, albeit with higher magnitude for the high-resolution case (Figs. 5a, b and 6a, b). For example, the decrease in XCO_2 is around 2 ppm in the low-resolution simulation, and around 10 ppm in the high-resolution simulation. The XCH_4 decrease is not as uniform as in XCO_2, being larger in the Northern Hemisphere mid-latitudes by approximately 10 ppb at high resolution. On the other hand, the Bermejo–Conde mass fixer removes even more mass in the Northern Hemisphere than in the Southern Hemisphere, particulary at high resolution (see Figs. 5c, d and 6c, d). This is a desirable effect, since the conservation error is expected to

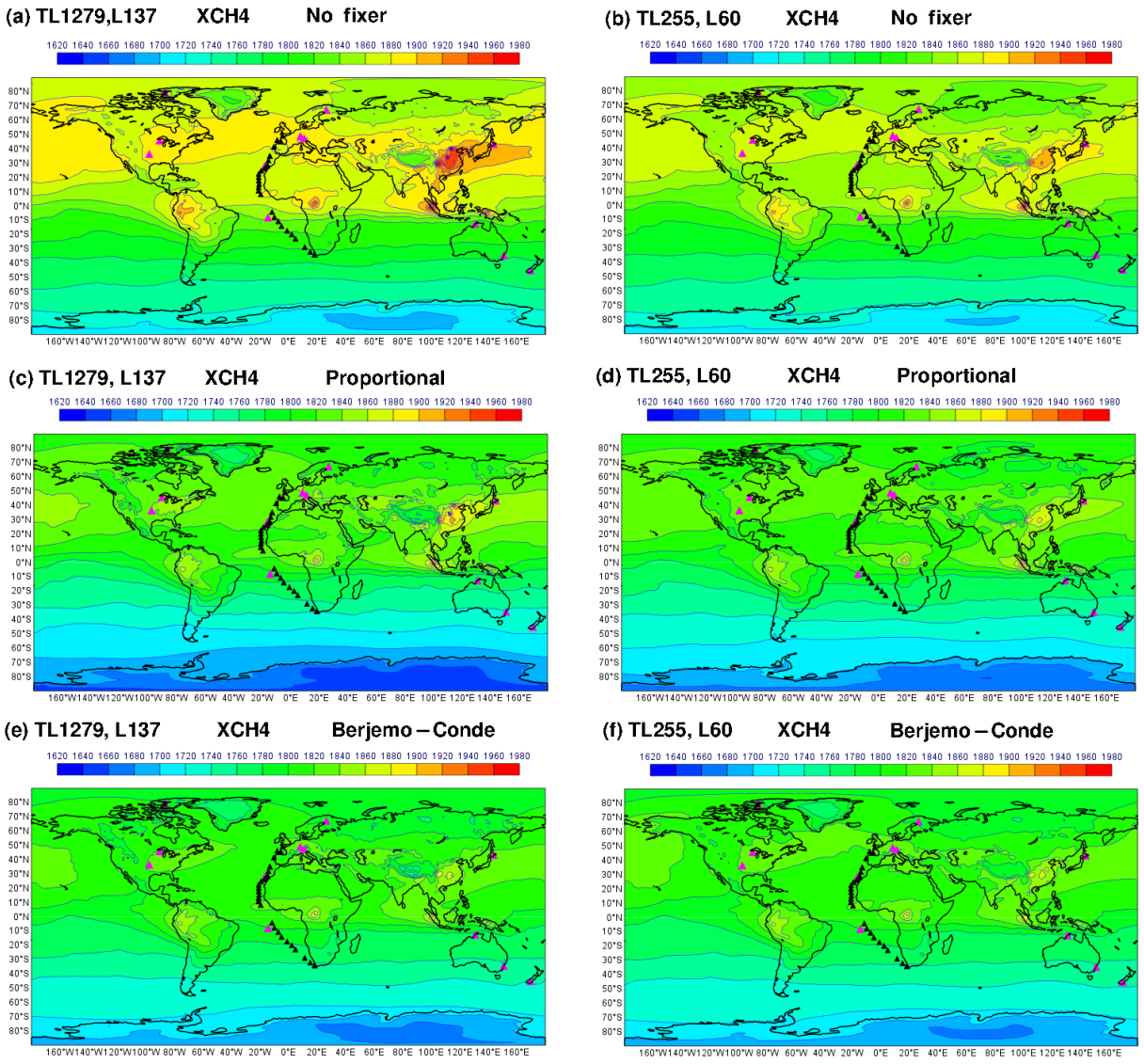

Figure 4. Mean XCH_4 (ppb) from 7 March to 10 April 2014 for the high-resolution (left panels) and low-resolution (right panels) simulations. The effect of the different mass fixers is shown in the different rows. Details of the simulations can be found in Table 1. The pink and black triangles mark the location of the reference observations from TCCON and *Polarstern* cruise respectively. See Table 2 for a list of the TCCON site coordinates.

be larger closer to the sources and/or sinks in the Northern Hemisphere.

5.3 Evaluation of inter-hemispheric gradient with observations

Comparing the simulations to the observed north–south transect in March–April 2014 we see that all the model simulations can represent the sign of the XCO_2 and XCH_4 gradient with larger values in the Northern Hemisphere and lower in the Southern Hemisphere (see Figs. 7 and 8).

The errors with respect to both TCCON and *Polarstern*-observed gradients are shown in Figs. 9 and 10. The gradient of both XCO_2 and XCH_4 is steepest at high resolution without the mass fixer, compared to the lower-resolution simulation and also to other simulations with the mass fixer. This corroborates the detrimental enhancement of XCO_2 and XCH_4 – particularly in the Northern Hemisphere – associated with the accumulation of mass conservation errors. The proportional mass fixer also results in a gradient which is too steep, particularly at high resolution (see light blue line in Figs. 7 and 8). The simulation with the Bermejo–Conde fixer has the gradient closest to the observed profiles. It also presents the best consistency (i.e. smallest difference) between high- and low-resolution simulations.

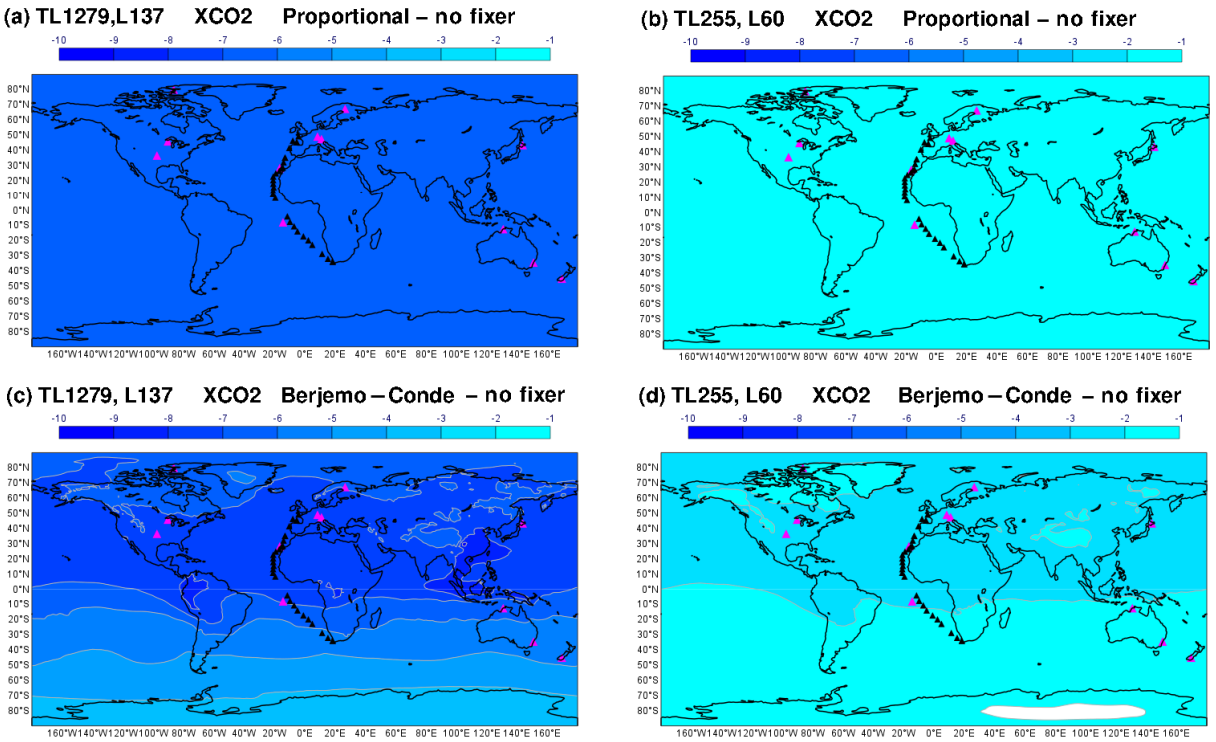

Figure 5. Difference in mean XCO_2 (ppm) between **(a, b)** the simulations using the proportional mass fixer and the simulation without mass fixer at high and low resolution respectively; **(c, d)** the simulation with Bermejo–Conde and the simulation without mass fixer at high and low resolutions respectively. The period covered and the marking of the observation sites are the same as in Fig. 3. See Table 2 for a list of the TCCON site coordinates.

Table 3. XCO_2 inter-hemispheric gradient (IHG) error (MODEL − OBS) statistics for simulations with different resolution and different mass fixers with respect to observations from the *Polarstern* cruise.

Data	IHG (ppm)	IHG error (ppm)	Overall bias (ppm) (%)	Inter-station bias (ppm) (%)
OBS	4.29			
Low resolution without fixer	7.81	3.52	2.70 (0.68)	1.54 (0.39)
Low resolution with proportional fixer	7.70	3.42	0.82 (0.21)	1.50 (0.38)
Low resolution with Bermejo–Conde	7.11	2.82	0.62 (0.16)	1.30 (0.33)
High resolution without fixer	10.54	6.25	7.86 (1.98)	2.54 (0.64)
High resolution with proportional fixer	10.17	5.89	1.36 (0.34)	2.40 (0.60)
High resolution with Bermejo–Conde	7.97	3.69	0.69 (0.17)	1.61 (0.40)
Spread of low-resolution simulations	0.70	0.70	2.01 (0.51)	0.24 (0.06)
Spread of high-resolution simulations	2.57	2.56	7.17 (1.81)	0.93 (0.24)
Spread of low-resolution Bermejo–Conde and proportional	0.59	0.60	0.20 (0.04)	0.20 (0.05)
Spread of high-resolution Bermejo–Conde and proportional	2.20	2.20	0.67 (0.17)	0.79 (0.20)

The inter-hemispheric gradient can be quantified as the difference between the tracer in the Northern Hemisphere and Southern Hemisphere. Here we take between 20 and 50° N and between 20 and 40° S for the two hemispheres due to the availability of observations. For XCO_2 the observed difference is 4.29 and 5.76 ppm using the *Polarstern* and the TCCON datasets respectively. For XCH_4 the gradient is 53.81 and 52.64 ppb for the same datasets respectively. The gradient for the different experiments is shown in Tables 3 to 6. All the low-resolution simulations have a similar gradient of XCO_2 of approximately 7 ppm with a range of 0.7 ppm (*Polarstern*) and 0.6 ppm (TCCON). That is, the range of

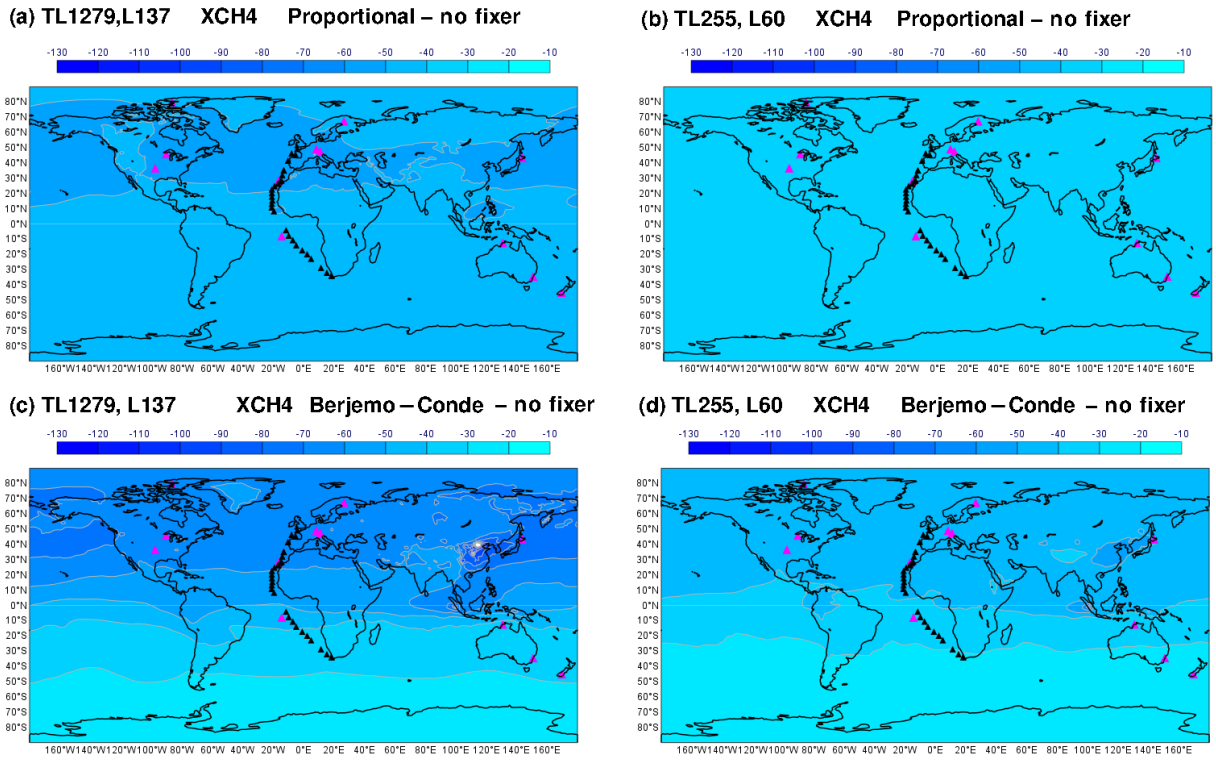

Figure 6. Difference in mean XCH_4 (ppb) between **(a, b)** the simulations using the proportional mass fixer and the simulation without mass fixer at high and low resolution respectively; **(c, d)** the simulation with Bermejo–Conde and the simulation without mass fixer at high and low resolutions respectively. The period covered and the marking of the observation sites are the same as in Fig. 4. See Table 2 for a list of the TCCON site coordinates.

Table 4. XCO_2 inter-hemispheric gradient (IHG) error (MODEL − OBS) statistics for simulations with different resolution and different mass fixers with respect to observations from TCCON.

Data	IHG (ppm)	IHG error (ppm)	Overall bias (ppm) (%)	Inter-station bias (ppm) (%)
OBS	5.76			
Low resolution without fixer	7.48	1.71	2.71 (0.68)	1.21 (0.30)
Low resolution with proportional fixer	7.45	1.68	0.83 (0.21)	1.20 (0.30)
Low resolution with Bermejo–Conde	6.93	1.16	0.69 (0.17)	1.02 (0.26)
High resolution without fixer	10.14	4.38	7.94 (1.99)	2.16 (0.54)
High resolution with proportional fixer	10.04	4.28	1.44 (0.36)	2.13 (0.54)
High resolution with Bermejo–Conde	8.10	2.34	0.88 (0.22)	1.45 (0.37)
Spread of low-resolution simulations	0.55	0.55	2.02 (0.51)	0.19 (0.05)
Spread of high-resolution simulations	2.04	2.04	7.06 (1.77)	0.71 (0.17)
Spread of low-resolution Bermejo–Conde and proportional	0.52	0.52	0.14 (0.04)	0.18 (0.05)
Spread of high-resolution Bermejo–Conde and proportional	1.94	1.94	0.56 (0.14)	0.68 (0.17)

inter-hemispheric gradients at the low resolution is around 10 % of its value, whereas the high-resolution simulations have a larger range of 2 ppm corresponding to a 30 % spread. This highlights the distorting effect of the mass conservation error on the inter-hemispheric gradient. For XCH_4 the effect is similar, albeit even more pronounced than for XCO_2 in the low-resolution simulations, where the range of the inter-hemispheric gradient values is around 18 ppb (i.e. 34 % of its value). At high resolution the XCH_4 range is around 34 ppb (i.e. 63 %).

When looking at the impact of each fixer, we see that the simulation with the proportional mass fixer has the same er-

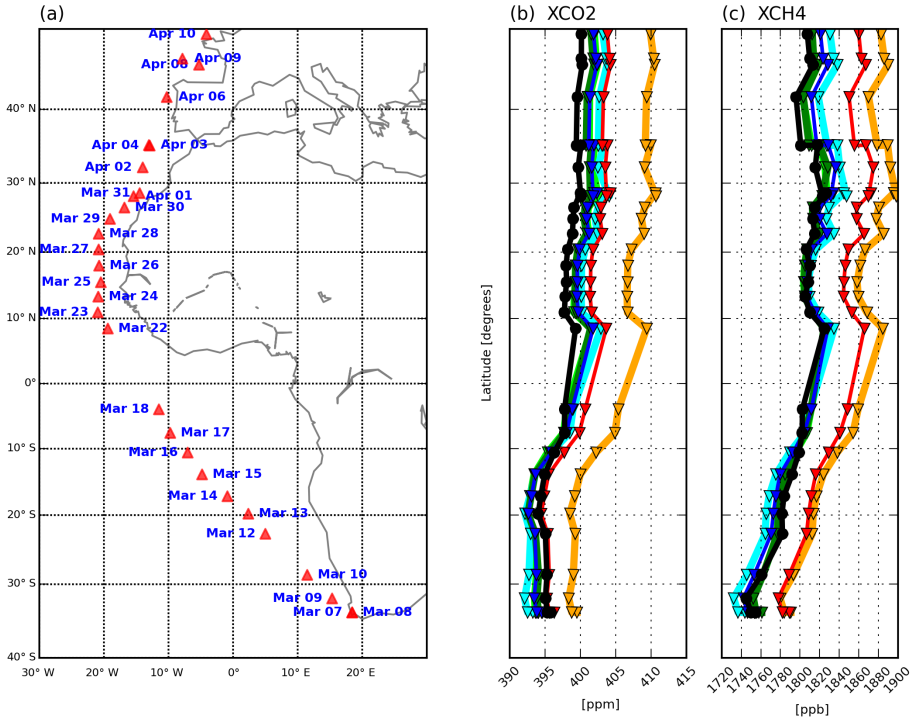

Figure 7. (a) Map showing the daily mean sampling location of *Polarstern* cruise. **(b, c)** Comparisons of latitudinal distribution of XCO_2 and XCH_4 as derived from monthly mean (7 March to 10 April) *Polarstern* observations (black) and simulations using different mass fixers at different resolutions: red and orange lines denote without mass fixer at low and high resolutions respectively; blue and cyan lines with the proportional mass fixer at low and high resolutions respectively; and green and light green with the Bermejo–Conde fixer and low and high resolutions respectively. See Table 1 for a more detailed description of the experiments.

Table 5. XCH_4 inter-hemispheric gradient (IHG) error (MODEL − OBS) statistics for simulations with different resolution and different mass fixers with respect to observations from the *Polarstern* cruise.

Data	IHG (ppb)	IHG error (ppb)	Overall bias (ppb) (%)	Inter-station bias (ppb) (%)
OBS	53.81			
Low resolution without fixer	73.42	19.61	41.09 (2.28)	9.88 (0.55)
Low resolution with proportional fixer	70.65	16.84	1.74 (0.10)	8.91 (0.50)
Low resolution with Bermejo–Conde	54.29	0.48	6.58 (0.37)	4.84 (0.27)
High resolution without fixer	92.00	38.19	55.83 (3.10)	16.84 (0.94)
High resolution with proportional fixer	88.19	34.38	6.05 (0.34)	15.36 (0.85)
High resolution with Bermejo–Conde	55.71	1.90	1.82 (0.10)	4.64 (0.26)
Spread of low-resolution simulations	19.13	19.13	39.35 (2.18)	5.05 (0.28)
Spread of high-resolution simulations	36.29	36.29	54.01 (3.00)	12.20 (0.68)
Spread of low-resolution Bermejo–Conde and proportional	16.36	16.36	2.01 (0.11)	4.07 (0.23)
Spread of high-resolution Bermejo–Conde and proportional	33.90	32.48	4.23 (0.24)	10.72 (0.59)

ror in inter-hemispheric gradient as the simulation without mass fixer (i.e. 4.3 to 5.9 ppm at high resolution and 1.6 to 3.4 ppm at low resolution, comprising 75 to 140 % of the error at high resolution and 32 to 79 % at low resolution). It is clear that the error grows with high resolution. This goes against all expectations as the objective of high-resolution simulations is to achieve a better accuracy. On the other hand, the Bermejo–Conde fixer is able to keep a closer gradient between the low- and high-resolution simulations (within 1 ppm and 2 ppb for XCO_2 and XCH_4). The resulting error with respect to both *Polarstern* and TCCON is nearly half the inter-hemispheric error of the proportional mass fixer.

Table 6. XCH_4 inter-hemispheric gradient (IHG) error (MODEL − OBS) statistics for simulations with different resolution and different mass fixers with respect to observations from TCCON.

Data	IHG (ppb)	IHG error (ppb)	Overall bias (ppb) (%)	Inter-station bias (ppb) (%)
OBS	52.64			
Low resolution without fixer	77.54	24.90	52.28 (2.92)	14.17 (0.79)
Low resolution with proportional fixer	76.06	23.42	14.77 (0.83)	13.76 (0.77)
Low resolution with Bermejo–Conde	60.96	8.32	11.47 (0.64)	9.02 (0.50)
High resolution without fixer	91.62	38.98	66.68 (3.72)	18.76 (1.05)
High resolution with proportional fixer	89.64	37.00	16.70 (0.93)	18.16 (1.01)
High resolution with Bermejo–Conde	59.78	7.14	9.90 (0.55)	7.62 (0.43)
Spread of low-resolution simulations	16.58	16.58	40.81 (2.28)	5.15 (0.29)
Spread of high-resolution simulations	31.84	31.84	56.78 (3.17)	11.14 (0.62)
Spread of low-resolution Bermejo–Conde and proportional	15.10	15.10	3.30 (1.19)	4.74 (0.27)
Spread of high-resolution Bermejo–Conde and proportional	29.86	29.86	6.80 (0.38)	10.54 (0.58)

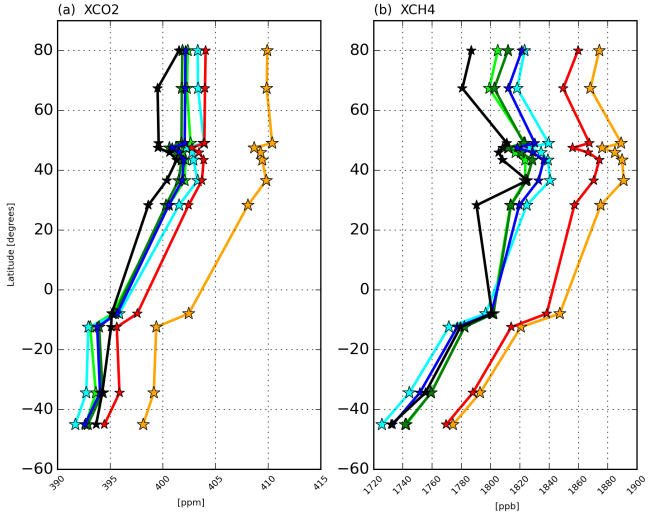

Figure 8. Comparisons of latitudinal distribution of **(a)** XCO_2 and **(b)** XCH_4 as derived from monthly mean (7 March to 10 April) TCCON sites (black, see Table 2) and simulations using different mass fixers at different resolutions: red and orange without mass fixer at low and high resolutions respectively; blue and cyan with the proportional mass fixer at low and high resolutions respectively; and green and light green with the Bermejo–Conde fixer and low and high resolutions respectively. See Table 1 for a more detailed description of the experiments.

These results are consistent with the station-to-station bias, which is computed as the standard deviation of the biases from the individual stations or cruise observations. The results are very similar when either there is no mass fixer or the proportional fixer mass is used. For XCO_2 the inter-station bias is 2 and 1.2 ppm at high and low resolutions respectively. However, for XCH_4 the inter-station bias ranges from 14 to 19 ppb and from 9 to 14 ppb at high and low resolutions respectively. The Bermejo–Conde is again showing an improvement with similar values for the high- and low-resolution simulations of around 1.4 ppm for XCO_2 and around 4.8 ppb for XCH_4. These values are in line with the variability of the bias in space and time obtained from satellite retrievals of GOSAT (Dils et al., 2014).

The effect of both proportional and Bermejo–Conde mass fixers on the bias with respect to observations is similar. They both manage to reduce the bias from around 2 % to less than 0.4 % for XCO_2 and from around 4 % to less than 1 % for XCH_4. It is worth noting that even for the bias, the Bermejo–Conde is able to have a reduction of the bias error of at least 0.1 % with respect to the proportional mass fixer, leading to an overall bias of 0.2 % ($\sim$ 0.7 ppm).

It is also remarkable that the resulting errors associated with the inter-hemispheric gradient are the same when using TCCON and *Polarstern* observations, despite being at different sampling sites (i.e. along different longitudes). The uniformity of the results throughout the globe means that the main error source is global. This is consistent with global error source of the mass fixer. Therefore, it strengthens the suggestion that the observations used here are able to detect the effects of the mass fixer more than the other effects associated with localised error sources from local fluxes and/or regional transport.

6 Conclusions

Atmospheric transport schemes used in models to monitor and/or predict climate change and atmospheric composition are required to conserve the global mass of atmospheric tracers. Thus, the use of numerical methods that do not inherently conserve mass, such as the widely used semi-Lagrangian advection scheme, entail the application of mass fixers to en-

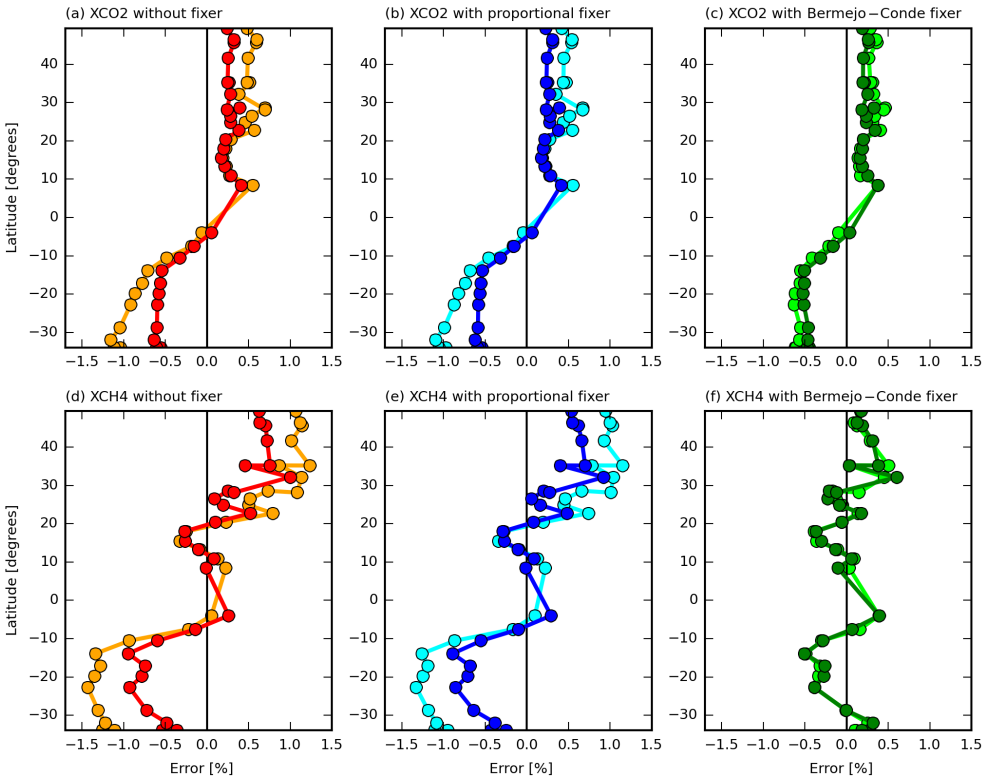

Figure 9. Error (%) of modelled latitudinal monthly mean (7 March to 10 April) distribution computed as (MODEL − OBS)/OBS using different tracer mass fixers and different resolutions for **(a–c)** XCO_2 and **(d–f)** XCH_4 with respect to the observed distribution from *Polarstern*. Dark and light colours correspond to the simulations at low and high resolution respectively.

sure the preservation of the global mass. This is particularly important for long-lived greenhouse gases for which the interesting signals to monitor (e.g. annual growth rates and large-scale spatial gradients) are weak compared to their background values. This paper explores the impact of two global mass fixers on the inter-hemispheric gradient of total column-averaged CO_2 and CH_4 using observations from the *Polarstern* cruise and the TCCON. The widely used proportional fixer is compared to the Bermejo–Conde fixer, presenting a feasible alternative in the context of operational atmospheric transport models.

Two different resolutions are also compared, the first one is a typical climate resolution of 80 km and 60 model levels and the second one is the current resolution used in NWP at 16 km in the horizontal and 137 model levels. Results clearly show that errors accumulate much faster for the high-resolution simulations and after 1 year the mass conservation error exceeds by far the observed annual growth rate of CO_2 and CH_4. The mass conservation errors of XCO_2 and XCH_4 grow faster in the Northern Hemisphere than in the Southern Hemisphere, causing a steepening of the inter-hemispheric gradient. The proportional mass fixer applies a uniform correction globally because it only depends on the background value which is uniformly high. Thus, the proportional fixer is efficient at removing the global bias, but it cannot correct for the steepening of the inter-hemispheric gradient. This is detected as an artificial reduction of XCO_2 and XCH_4 in the Southern Hemisphere and a resulting excess in the Northern Hemisphere when comparing with observations as depicted in Fig. 11. On the other hand, the alternative Bermejo–Conde fixer enhances the mass correction in the regions where gradients are steeper. CO_2 and CH_4 gradients are steeper where their surface fluxes are stronger, i.e. in the Northern Hemisphere. The Bermejo–Conde mass fixer correction is therefore latitudinally dependent and it is able to correct the inter-hemispheric gradient, bringing the low- and high-resolution simulations closer to each other and closer to the observations.

In summary, the tests performed using the IFS show that although the proportional mass fixer is suitable at low resolutions currently used in NWP re-analysis and climate simulations, it is not suitable for NWP resolutions at 16 km and 137 vertical levels. An alternative global mass fixer based on Bermejo–Conde has been shown to work reasonably well when compared to observations at both low and high resolutions without too much additional complexity or cost.

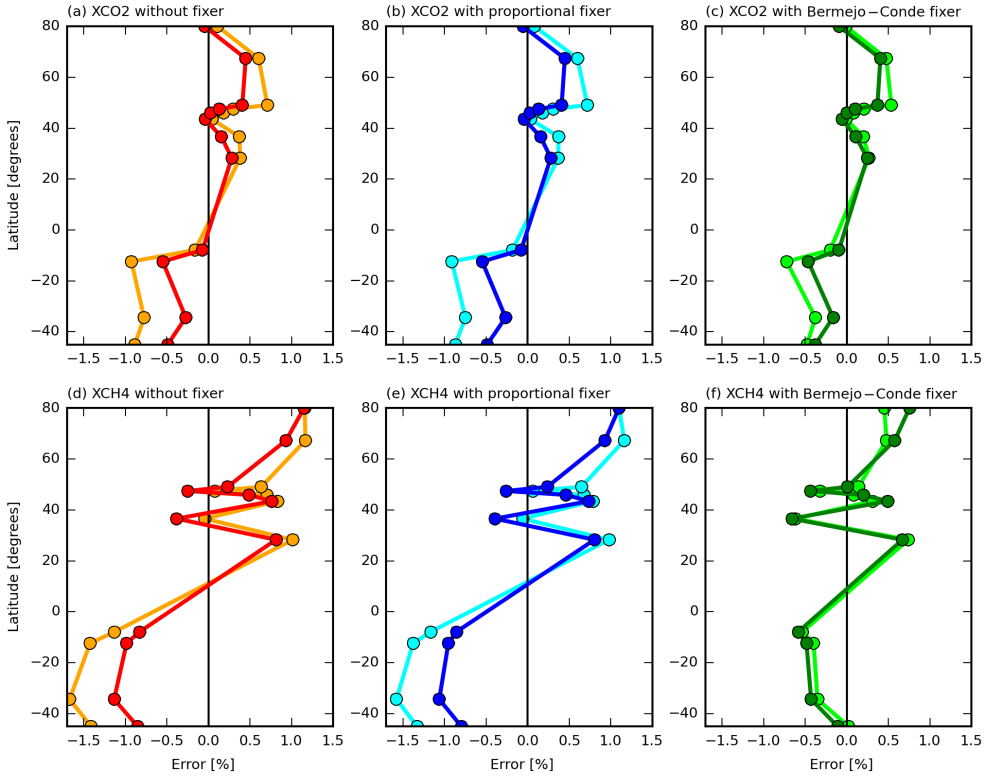

Figure 10. Error (%) of modelled latitudinal monthly mean (7 March to 10 April) distribution computed as (MODEL − OBS)/OBS using different tracer mass fixers and different resolutions for **(a–c)** XCO_2 and **(d–f)** XCH_4 with respect to the observed distribution from TCCON. Dark and light colours correspond to the simulations at low and high resolution respectively.

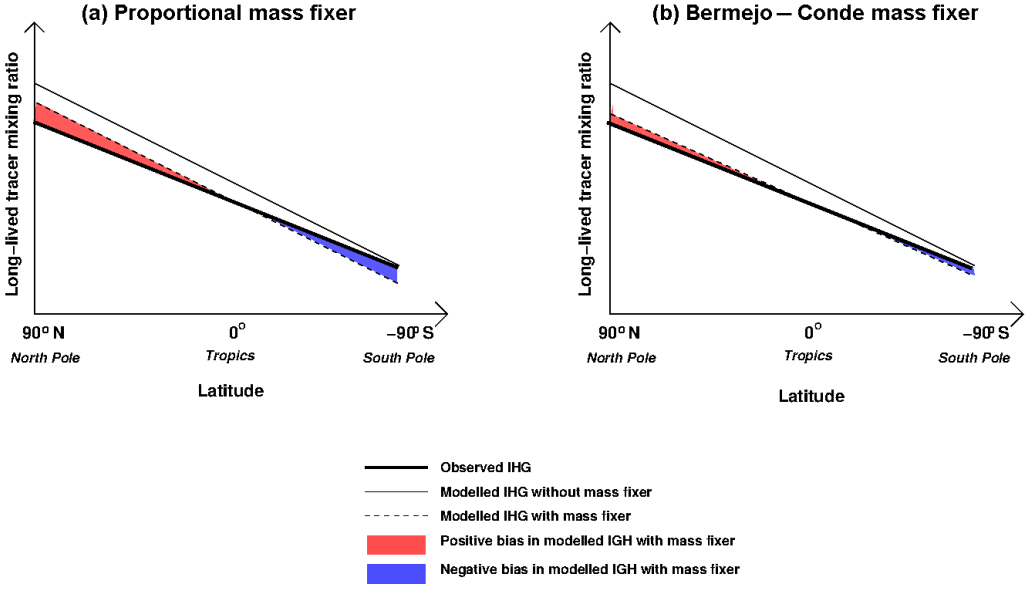

Figure 11. Schematic illustrating the impact of the **(a)** proportional and **(b)** Bermejo–Conde mass fixers on the inter-hemispheric gradient of XCO_2 and XCH_4. Note that the area between the dash line and thin solid line depicting the global correction of tracer mass should be the same for the two mass fixers.

7 Code and data availability

This particular study has been based on the IFS model cycle 41R2. The C-IFS source code is integrated into ECWMF's IFS code, which is only available subject to a licence agreement with ECMWF. ECMWF member-state weather services and their approved partners will get access granted. The IFS code without modules for assimilation and chemistry can be obtained for educational and academic purposes as part of the openIFS release (https://software.ecmwf.int/wiki/display/OIFS/OpenIFS+Home). A detailed documentation of the IFS code is available from https://software.ecmwf.int/wiki/display/IFS/CY40R1+Official+IFS+Documentation. The output from C-IFS can be requested via http://copernicus-support.ecmwf.int. The *Polarstern* data is available in the Supplement of Klappenbach et al. (2015) at doi:10.5194/amt-8-5023-2015-supplement. The TCCON data (version GGG2014) is available from tccon.ornl.gov.

Acknowledgements. This study has been funded by the European Commission under Monitoring of Atmospheric Composition and Climate project and the Copernicus Atmosphere Monitoring Service.

F. Klappenbach and A. Butz acknowledge support by Frank Hase, KIT, for instrument development and data reduction, by the Emmy Noether Programme of the Deutsche Forschungsgemeinschaft (DFG) through grant BU2599/1-1 (RemoteC), and by Alfred Wegener Institute (AWI), Helmholtz Centre for Polar and Marine Research, for operating RV *Polarstern* and granting access to its infrastructures.

TCCON data were obtained from the TCCON Data Archive, hosted by the Carbon Dioxide Information Analysis Center (CDIAC) – tccon.onrl.gov. The authors would like to acknowledge the PIs of the different TCCON stations used in this study: Kimberly Strong (Eureka, Canada) Rigel Kivi (Sodankylä, Finland), Frank Hase (Karlsruhe, Germany), Ralf Sussmann (Garmisch, Germany), Paul Wennberg (Park Falls, Lamont, USA), Matthias Schneider (Izaña, Spain), Dietrich Feist (Ascension Island), David Griffith (Darwin, Wollongong, Australia), Dave Pollard and Vanessa Sherlock (Lauder, New Zealand). The operation at the Rikubetsu TCCON site is supported in part by the budget from the GOSAT data validation project funded by the Ministry of Environment, Japan.

The authors are grateful to Sebastien Massart and Johannes Flemming for useful discussions and comments during the completion of this work.

Edited by: S. Remy
Reviewed by: two anonymous referees

References

Agustí-Panareda, A., Massart, S., Chevallier, F., Boussetta, S., Balsamo, G., Beljaars, A., Ciais, P., Deutscher, N. M., Engelen, R., Jones, L., Kivi, R., Paris, J.-D., Peuch, V.-H., Sherlock, V., Vermeulen, A. T., Wennberg, P. O., and Wunch, D.: Forecasting global atmospheric CO_2, Atmos. Chem. Phys., 14, 11959–11983, doi:10.5194/acp-14-11959-2014, 2014.

Agustí-Panareda, A., Massart, S., Chevallier, F., Balsamo, G., Boussetta, S., Dutra, E., and Beljaars, A.: A biogenic CO_2 flux adjustment scheme for the mitigation of large-scale biases in global atmospheric CO_2 analyses and forecasts, Atmos. Chem. Phys., 16, 10399–10418, doi:10.5194/acp-16-10399-2016, 2016.

Bechtold, P., Köhler, M., Jung, T., Doblas-Reyes, F., Leutbecher, M., Rodwell, M., Vitart, F., and Balsamo, G.: Advances in simulating atmospheric variability with the ECMWF model: From synoptic to decadal time-scales, Q. J. Roy. Meteor. Soc., 134, 1337–1351, 2008.

Bechtold, P., Semane, N., Lopez, P., Chaboureau, J.-P., Beljaars, A., and Bormann, N.: Representing equilibrium and nonequilibrium convection in large-scale models, J. Atmos. Sci., 71, 734–753, 2014.

Beljaars, A. and Viterbo, P.: The role of the boundary layer in a numerical weather prediction model, in: Clear and cloudy boundary layers, Royal Netherlands Academy of Arts and Sciences, North Holland Publishers, Amsterdam, 1998.

Bergamaschi, P., Frankenberg, C., Meirink, J. F., Krol, M., Villani, M. G., Houweling, S., Dentener, F., Dlugokencky, E. J., Miller, J. B., Gatti, L. V., Engel, A., and Levin, I.: Inverse modeling of global and regional CH_4 emissions using SCIAMACHY satellite retrievals, J. Geophys. Res., 114, D22301, doi:10.1029/2009JD012287, 2009.

Bermejo, R. and Conde, J.: A conservative Quasi-Monotone Semi-Lagrangian Scheme, Mon. Weather Rev., 130, 423–430, 2002.

Blumenstock, T., Hase, F., Schneider, M., García, O. E., and Sepúlveda, E.: TCCON data from Izana (ES), Release GGG2014R0, TCCON data archive, hosted by CDIAC, doi:10.14291/tccon.ggg2014.izana01.R0/1149295, 2014.

Boussetta, S., Balsamo, G., Beljaars, A., Agusti-Panareda, A., Calvet, J.-C., Jacobs, C., van den Hurk, B., Viterbo, P., Lafont, S., Dutra, E., Jarlan, L., Balzarolo, M., Papale, D., and van der Werf, G.: Natural carbon dioxide exchanges in the ECMWF Integrated Forecasting System: Implementation and offline validation, J. Geophys. Res.-Atmos., 118, 1–24, doi:10.1002/jgrd.50488, 2013.

Butz, A., Guerlet, S., Hasekamp, O., Schepers, D., Galli, A., Aben, I., Frankenberg, C., Hartmann, J., Tran, H., Kuze, A., Keppel-Aleks, G., Toon, G., Wunch, D., Wennberg, P., Deutscher, N., Griffith, D., Macatangay, R., Messerschmidt, J., Notholt, J., and Warneke, T.: Toward accurate CO_2 and CH_4 observations from GOSAT, Geophys. Res. Lett., 38, L14812, doi:10.1029/2011GL047888, 2011.

Chevallier, F., Ciais, P., Conway, T., Aalto, T., Anderson, B., Bousquet, P., Brunke, E., Ciattaglia, L., Esaki, Y., Fröhlich, M., Gomez, A., Gomez-Pelaez, A., Haszpra, L., Krummel, P., Langenfelds, R., Leuenberger, M., Machida, T., Maignan, F., Matsueda, H., Morguí, J., Mukai, H., Nakazawa, T., Peylin, P., Ramonet, M., Rivier, L., Sawa, Y., Schmidt, M., Steele, L., Vay, S., Vermeulen, A., Wofsy, S., and Worthy, D.: CO_2 surface fluxes at grid point scale estimated from a global 21 year reanalysis

of atmospheric measurements, J. Geophys. Res., 115, D21307, doi:10.1029/2010JD013887, 2010.

Collins, W. J., Bellouin, N., Doutriaux-Boucher, M., Gedney, N., Halloran, P., Hinton, T., Hughes, J., Jones, C. D., Joshi, M., Liddicoat, S., Martin, G., O'Connor, F., Rae, J., Senior, C., Sitch, S., Totterdell, I., Wiltshire, A., and Woodward, S.: Development and evaluation of an Earth-System model – HadGEM2, Geosci. Model Dev., 4, 1051–1075, doi:10.5194/gmd-4-1051-2011, 2011.

Corbin, K. and Law, R.: Extending atmospheric CO_2 and tracer capabilities in ACCESS, Tech. rep., Centre for Australian Weather and Climate Research, Australia, available at: http://www.cawcr.gov.au/technical-reports/CTR_035.pdf (last access: 21 December 2016), 2011.

Dargaville, R., Doney, S., and Fung, I.: Inter-annual variability in the interhemispheric atmospheric CO_2 gradient: contributions from transport and the seasonal rectifier, Tellus, 55B, 711–722, 2003.

de Grandpré, J., Tanguay, M., Qaddouri, A., Zerroukat, M., and McLinden, C.: Semi-Lagrangian Advection of Stratospheric Ozone on a Yin-Yang Grid System, Mon. Weather Rev., 144, 1035–1050, doi:10.1175/MWR-D-15-0142.1, 2016.

Diamantakis, M. and Flemming, J.: Global mass fixer algorithms for conservative tracer transport in the ECMWF model, Geosci. Model Dev., 7, 965–979, doi:10.5194/gmd-7-965-2014, 2014.

Dils, B., Buchwitz, M., Reuter, M., Schneising, O., Boesch, H., Parker, R., Guerlet, S., Aben, I., Blumenstock, T., Burrows, J. P., Butz, A., Deutscher, N. M., Frankenberg, C., Hase, F., Hasekamp, O. P., Heymann, J., De Mazière, M., Notholt, J., Sussmann, R., Warneke, T., Griffith, D., Sherlock, V., and Wunch, D.: The Greenhouse Gas Climate Change Initiative (GHG-CCI): comparative validation of GHG-CCI SCIAMACHY/ENVISAT and TANSO-FTS/GOSAT CO_2 and CH_4 retrieval algorithm products with measurements from the TCCON, Atmos. Meas. Tech., 7, 1723–1744, doi:10.5194/amt-7-1723-2014, 2014.

Dlugokencky, E. J., Bruhwiler, L., White, J. W. C., Emmons, L. K., Novelli, P. C., Montzka, S. A., Masarie, K. A., Lang, P. M., Crotwell, A. M., Miller, J. B., and Gatti, L. V.: Observational constraints on recent increases in the atmospheric CH_4 burden, Geophys. Res. Lett., 36, L18803, doi:10.1029/2009GL039780, 2009.

Feist, D. G., Arnold, S. G., John, N., and Geibel, M. C.: TCCON data from Ascension Island (SH), Release GGG2014R0, TCCON data archive, hosted by CDIAC, doi:10.14291/tccon.ggg2014.ascension01.R0/1149285, 2014.

Flemming, J., Huijnen, V., Arteta, J., Bechtold, P., Beljaars, A., Blechschmidt, A.-M., Diamantakis, M., Engelen, R. J., Gaudel, A., Inness, A., Jones, L., Josse, B., Katragkou, E., Marecal, V., Peuch, V.-H., Richter, A., Schultz, M. G., Stein, O., and Tsikerdekis, A.: Tropospheric chemistry in the Integrated Forecasting System of ECMWF, Geosci. Model Dev., 8, 975–1003, doi:10.5194/gmd-8-975-2015, 2015.

Forster, P., Ramaswamy, V., Artaxo, P., Berntsen, T., Betts, R., Fahey, D., Haywood, J., Lean, J., Lowe, D., Myhre, G., Nganga, J., Prinn, R., Raga, G., Schulz, M., and Dorland, R. V.: Changes in Atmospheric Constituents and in Radiative Forcing, in: Climate Change 2007: The Physical Science Basis. Contribution of Working Group I to the Fourth Assessment Report of the Intergovernmental Panel on Climate Change, edited by: Solomon, S., Qin, D., Manning, M., Chen, Z., Marquis, M., Averyt, K. B., Tignor, M., and Miller, H. L., Cambridge University Press, Cambridge, United Kingdom and New York, NY, USA, 2007.

Frey, M., Hase, F., Blumenstock, T., Groß, J., Kiel, M., Mengistu Tsidu, G., Schäfer, K., Sha, M. K., and Orphal, J.: Calibration and instrumental line shape characterization of a set of portable FTIR spectrometers for detecting greenhouse gas emissions, Atmos. Meas. Tech., 8, 3047–3057, doi:10.5194/amt-8-3047-2015, 2015.

Gisi, M., Hase, F., Dohe, S., Blumenstock, T., Simon, A., and Keens, A.: XCO_2-measurements with a tabletop FTS using solar absorption spectroscopy, Atmos. Meas. Tech., 5, 2969–2980, doi:10.5194/amt-5-2969-2012, 2012.

Griffith, D. W. T., Deutscher, N., Velazco, V. A., Wennberg, P. O., Yavin, Y., Aleks, G. K., Washenfelder, R., Toon, G. C., Blavier, J.-F., Murphy, C., Jones, N., Kettlewell, G., Connor, B., Macatangay, R., Roehl, C., Ryczek, M., Glowacki, J., Culgan, T., and Bryant, G.: TCCON data from Darwin (AU), Release GGG2014R0, TCCON data archive, hosted by CDIAC, doi:10.14291/tccon.ggg2014.darwin01.R0/1149290, 2014.

Griffith, D. W. T., Velazco, V. A., Deutscher, N., Murphy, C., Jones, N., Wilson, S., Macatangay, R., Kettlewell, G., Buchholz, R. R., and Riggenbach, M.: TCCON data from Wollongong (AU), Release GGG2014R0, TCCON data archive, hosted by CDIAC, doi:10.14291/tccon.ggg2014.bialystok01.R0/1149277, 2014.

Gurney, K., Law, R., Denning, A., Rayner, P., Baker, D., Bousquet, P., Bruhwiler, L., Chen, Y.-H., Ciais, P., Fan, S., Fung, I., Gloor, M., Heimann, M., Higuchi, K., John, J., Maki, T., Maksyutov, S., Masarie, K., Peylin, P., Prather, M., Pak, B., Randerson, J., Sarmiento, J., Taguchi, S., Takahashi, T., and Yuen, C.-W.: Towards robust regional estimates of CO_2 sources and sinks using atmospheric transport models, Nature, 415, 626–630, 2002.

Hase, F., Blumenstock, T., Dohe, S., Gross, J., and Kiel, M.: TCCON data from Karlsruhe (DE), Release GGG2014R1, TCCON data archive, hosted by CDIAC, doi:10.14291/tccon.ggg2014.karlsruhe01.R1/1182416, 2014.

Hase, F., Frey, M., Blumenstock, T., Groß, J., Kiel, M., Kohlhepp, R., Mengistu Tsidu, G., Schäfer, K., Sha, M. K., and Orphal, J.: Application of portable FTIR spectrometers for detecting greenhouse gas emissions of the major city Berlin, Atmos. Meas. Tech., 8, 3059–3068, doi:10.5194/amt-8-3059-2015, 2015.

Hortal, M.: The development and testing of a new two-time-level semi-Lagrangian scheme (SETTLS) in the ECMWF forecast model, Q. J. Roy. Meteor. Soc., 128, 1671–1687, doi:10.1002/qj.200212858314, 2002.

Houweling, S., Aben, I., Breon, F.-M., Chevallier, F., Deutscher, N., Engelen, R., Gerbig, C., Griffith, D., Hungershoefer, K., Macatangay, R., Marshall, J., Notholt, J., Peters, W., and Serrar, S.: The importance of transport model uncertainties for the estimation of CO_2 sources and sinks using satellite measurements, Atmos. Chem. Phys., 10, 9981–9992, doi:10.5194/acp-10-9981-2010, 2010.

Jöckel, P., von Kuhlmann, R., Lawrence, M. G., Steil, B., Brenninkmeuer, C. A. M., Crutzen, P. J., Rasch, P. J., and Eaton, B.: On a fundamental problem in implementing flux-form advection schemes for tracer transport in 3-dimensional general circulation and chemistry transport models, Q. J. Roy. Meteor. Soc., 127, 1035–1052, 2001.

Jones, C. D., Hughes, J. K., Bellouin, N., Hardiman, S. C., Jones, G. S., Knight, J., Liddicoat, S., O'Connor, F. M., Andres, R. J., Bell, C., Boo, K.-O., Bozzo, A., Butchart, N., Cadule, P., Corbin, K. D., Doutriaux-Boucher, M., Friedlingstein, P., Gornall, J., Gray, L., Halloran, P. R., Hurtt, G., Ingram, W. J., Lamarque, J.-F., Law, R. M., Meinshausen, M., Osprey, S., Palin, E. J., Parsons Chini, L., Raddatz, T., Sanderson, M. G., Sellar, A. A., Schurer, A., Valdes, P., Wood, N., Woodward, S., Yoshioka, M., and Zerroukat, M.: The HadGEM2-ES implementation of CMIP5 centennial simulations, Geosci. Model Dev., 4, 543–570, doi:10.5194/gmd-4-543-2011, 2011.

Jones, C., Robertson, E., Arora, V., Friedlingstein, P., Shevliakove, E., Bopp, L., Brovkin, V., Hajima, T., Kato, E., Kawamiya, M., Liddicoat, S., Lindsay, K., Reick, C., Roelandt, C., Segschneider, J., and Tjiputra, J.: 21st Century compatible CO_2 emissions and airborne fraction simulated by CMIP5 Earth System models under 4 Representative Concentration Pathways, J. Climate, 26, 4398–4413, doi:10.1175/JCLI-D-12-00554.1, 2013.

Kaiser, J. W., Heil, A., Andreae, M. O., Benedetti, A., Chubarova, N., Jones, L., Morcrette, J.-J., Razinger, M., Schultz, M. G., Suttie, M., and van der Werf, G. R.: Biomass burning emissions estimated with a global fire assimilation system based on observed fire radiative power, Biogeosciences, 9, 527–554, doi:10.5194/bg-9-527-2012, 2012.

Keppel-Aleks, G., Wennberg, P., and Schneider, T.: Sources of variations in total column carbon dioxide, Atmos. Chem. Phys., 11, 3581–3593, doi:10.5194/acp-11-3581-2011, 2011.

Keppel-Aleks, G., Randerson, J., Lindsay, K., Stephens, B., Moore, J., Doney, S., Thornton, P., Mahowald, N., Hoffman, F., Sweeney, C., Tans, P., Wennberg, P., and Wofsy, S.: Atmospheric carbon dioxide variability in the Community Earth System Model: Evaluation and transient dynamic during the 20th and 21st centuries, J. Climate, 26, 4447–4475, doi:10.1175/JCLI-D-12-00589.1, 2013.

Kirschke, S., Bousquet, P., Ciais, P., Saunois, M., Canadell, J. G., Dlugokencky, E. J., Bergamaschi, P., Bergmann, D., Blake, D. R., Bruhwiler, L., Cameron-Smith, P., Castaldi, S., Chevallier, F., Feng, L., Fraser, A., Heimann, M., Hodson, E. L., Houweling, S., Josse, B., Fraser, P. J., Krummel, P. B., Lamarque, J.-F., Langenfelds, R. L., Quéré, C. L., Naik, V., O'Doherty, S., Palmer, P. I., Pison, I., Plummer, D., Poulter, B., Prinn, R. G., Rigby, M., Ringeval, B., Santini, M., Schmidt, M., Shindell, D. T., Simpson, I. J., Spahni, R., Steele, L. P., Strode, S. A., Sudo, K., Szopa, S., van der Werf, G. R., Voulgarakis, A., van Weele, M., Weiss, R. F., Williams, J. E., and Zeng, G.: Three decades of global methane sources and sinks, Nat. Geosci., 6, 813–823, doi:10.1038/ngeo1955, 2013.

Kivi, R., Heikkinen, P., and Kyrö, E.: TCCON data from Sodankylä (FI), Release GGG2014R0, TCCON data archive, hosted by CDIAC, doi:10.14291/tccon.ggg2014.sodankyla01.R0/1149280, 2014.

Klappenbach, F., Bertleff, M., Kostinek, J., Hase, F., Blumenstock, T., Agusti-Panareda, A., Razinger, M., and Butz, A.: Accurate mobile remote sensing of XCO_2 and XCH_4 latitudinal transects from aboard a research vessel, Atmos. Meas. Tech., 8, 5023–5038, doi:10.5194/amt-8-5023-2015, 2015.

Koehler, M., Ahlgrimm, M., and Beljaars, A.: Unified treatment of dry convective and stratocumulus-topped boundary layers in the ecmwf model, Q. J. Roy. Meteor. Soc., 137, 43–57, 2011.

Le Quéré, C., Moriarty, R., Andrew, R. M., Canadell, J. G., Sitch, S., Korsbakken, J. I., Friedlingstein, P., Peters, G. P., Andres, R. J., Boden, T. A., Houghton, R. A., House, J. I., Keeling, R. F., Tans, P., Arneth, A., Bakker, D. C. E., Barbero, L., Bopp, L., Chang, J., Chevallier, F., Chini, L. P., Ciais, P., Fader, M., Feely, R. A., Gkritzalis, T., Harris, I., Hauck, J., Ilyina, T., Jain, A. K., Kato, E., Kitidis, V., Klein Goldewijk, K., Koven, C., Landschützer, P., Lauvset, S. K., Lefèvre, N., Lenton, A., Lima, I. D., Metzl, N., Millero, F., Munro, D. R., Murata, A., Nabel, J. E. M. S., Nakaoka, S., Nojiri, Y., O'Brien, K., Olsen, A., Ono, T., Pérez, F. F., Pfeil, B., Pierrot, D., Poulter, B., Rehder, G., Rödenbeck, C., Saito, S., Schuster, U., Schwinger, J., Séférian, R., Steinhoff, T., Stocker, B. D., Sutton, A. J., Takahashi, T., Tilbrook, B., van der Laan-Luijkx, I. T., van der Werf, G. R., van Heuven, S., Vandemark, D., Viovy, N., Wiltshire, A., Zaehle, S., and Zeng, N.: Global Carbon Budget 2015, Earth Syst. Sci. Data, 7, 349–396, doi:10.5194/essd-7-349-2015, 2015.

Locatelli, R., Bousquet, P., Chevallier, F., Fortems-Cheney, A., Szopa, S., Saunois, M., Agusti-Panareda, A., Bergmann, D., Bian, H., Cameron-Smith, P., Chipperfield, M. P., Gloor, E., Houweling, S., Kawa, S. R., Krol, M., Patra, P. K., Prinn, R. G., Rigby, M., Saito, R., and Wilson, C.: Impact of transport model errors on the global and regional methane emissions estimated by inverse modelling, Atmos. Chem. Phys., 13, 9917–9937, doi:10.5194/acp-13-9917-2013, 2013.

Maksyutov, S., Patra, P., Onishi, R., Saeki, T., and Nakazawa, T.: NIES/FRCGC Global Atmospheric Tracer Transport Model: Description, Validation, and Surface Sources and Sinks Inversion, J. Earth Simulator, 9, 3–18, 2008.

Massart, S., Agusti-Panareda, A., Aben, I., Butz, A., Chevallier, F., Crevoisier, C., Engelen, R., Frankenberg, C., and Hasekamp, O.: Assimilation of atmospheric methane products into the MACC-II system: from SCIAMACHY to TANSO and IASI, Atmos. Chem. Phys., 14, 6139–6158, doi:10.5194/acp-14-6139-2014, 2014.

Massart, S., Agusti-Panareda, A., Heymann, J., Buchwitz, M., Chevallier, F., Reuter, M., Hilker, M., and Burrows, J.: Ability of the 4D-Var analysis of the GOSAT BESD XCO_2 retrievals to characterize atmospheric CO_2 at large and synoptic scales, Atmos. Chem. Phys., 16, 1653–1671, doi:10.5194/acp-16-1653-2016, 2016.

Morino, I., Yokozeki, N., Matzuzaki, T., Ikegami, H., and Shishime, A.: TCCON data from Rikubetsu (JP), Release GGG2014R1, TCCON data archive, hosted by CDIAC, doi:10.14291/tccon.ggg2014.rikubetsu01.R0/1149282, 2014.

Oshchepkov, S., Bril, A., Yokota, T., Wennberg, P., Deutscher, N., Wunch, D., Toon, G., Yoshida, Y., O'Dell, C., Crisp, D., Miller, C., Frankenberg, C., Butz, A., Aben, I., Guerlet, S., Hasekamp, O., Boesch, H., Cogan, A., Parker, R., Griffith, D., Macatangay, R., Notholt, J., Sussmann, R., Rettinger, M., Sherlock, V., Robinson, J., Kyrö, E., Heikkinen, P., Feist, D., Morino, I., Kadygrov, N., Maksuytov, D. B. S., Matsunaga, T., Uchino, O., and Watanabe, H.: Effects of atmospheric light scattering on spectroscopic observations of greenhouse gases from space. Part 2: Algorithm intercomparison in the GOSAT data processing for CO_2 retrievals over TCCON sites, J. Geophys. Res.-Atmos., 118, 1493–1512, doi:10.1002/jgrd.50146, 2013.

Patra, P. K., Houweling, S., Krol, M., Bousquet, P., Belikov, D., Bergmann, D., Bian, H., Cameron-Smith, P., Chipperfield, M. P., Corbin, K., Fortems-Cheiney, A., Fraser, A., Gloor, E., Hess, P.,

Ito, A., Kawa, S. R., Law, R. M., Loh, Z., Maksyutov, S., Meng, L., Palmer, P. I., Prinn, R. G., Rigby, M., Saito, R., and Wilson, C.: TransCom model simulations of CH_4 and related species: linking transport, surface flux and chemical loss with CH_4 variability in the troposphere and lower stratosphere, Atmos. Chem. Phys., 11, 12813–12837, doi:10.5194/acp-11-12813-2011, 2011.

Polavarapu, S. M., Neish, M., Tanguay, M., Girard, C., de Grandpré, J., Semeniuk, K., Gravel, S., Ren, S., Roche, S., Chan, D., and Strong, K.: Greenhouse gas simulations with a coupled meteorological and transport model: the predictability of CO_2, Atmos. Chem. Phys., 16, 12005–12038, doi:10.5194/acp-16-12005-2016, 2016.

Rodgers, C. and Connor, B.: Intercomparison of remote sounding instruments, J. Geophys. Res., 108, D3, doi:10.1029/2002JD002299, 2003.

Saito, R., Patra, P. K., Deutscher, N., Wunch, D., Ishijima, K., Sherlock, V., Blumenstock, T., Dohe, S., Griffith, D., Hase, F., Heikkinen, P., Kyrö, E., Macatangay, R., Mendonca, J., Messerschmidt, J., Morino, I., Notholt, J., Rettinger, M., Strong, K., Sussmann, R., and Warneke, T.: Technical Note: Latitude-time variations of atmospheric column-average dry air mole fractions of CO_2, CH_4 and N_2O, Atmos. Chem. Phys., 12, 7767–7777, doi:10.5194/acp-12-7767-2012, 2012.

Saito, R., Patra, P., Sweeney, C., Machida, T., Krol, M., Houweling, S., Bousquet, P., Agusti-Panareda, A., Belikov, D., Bergmann, D., Bian, H., Cameron-Smith, P., Chipperfield, M., Fortems-Cheiney, A., Fraser, A., Gatti, L., Gloor, E., Hess, P., Kawa, S., Law, R., Locatelli, R., Loh, Z., Maksyutov, S., Meng, L., Miller, J., Palmer, P., Prinn, R., Rigby, M., and Wilson, C.: TransCom model simulations of methane: comparison of vertical profiles with aircraft measurements, J. Geophys. Res., 118, 1–14, doi:10.1002/jgrd.50380, 2013.

Sandu, I., Beljaars, A., Bechtold, P., Mauritsen, T., and Balsamo, G.: Why is it so difficult to represent stably stratified conditions in numerical weather prediction (NWP) models?, J. Adv. Model. Earth Syst., 5, 1–17, doi:10.1002/jame.20013, 2013.

Sherlock, V. B., Connor, Robinson, J., Shiona, H., Smale, D., and Pollard, D.: TCCON data from Lauder (NZ), 125HR, Release GGG2014R0, TCCON data archive, hosted by CDIAC, doi:10.14291/tccon.ggg2014.lauder02.R0/1149298, 2014.

Strong, K., Mendonca, J., Weaver, D., Fogal, P., Drummond, J., Batchelor, R., and Lindenmaier, R.: TCCON data from Eureka (CA), Release GGG2014R0, TCCON data archive, hosted by CDIAC, doi:10.14291/tccon.ggg2014.eureka01.R0/1149271, 2014.

Sussmann, R. and Rettinger, M.: TCCON data from Garmisch (DE), Release GGG2014R0, TCCON data archive, hosted by CDIAC, doi:10.14291/tccon.ggg2014.garmisch01.R0/1149299, 2014.

Temperton, C., Hortal, M., and Simmons, A.: A two-time-level semi-Lagrangian global spectral model, Q. J. Roy. Meteor. Soc., 127, 111–126, 2001.

Tiedtke, M.: A comprehensive mass flux scheme for cumulus parameterization in large-scale models, Mon. Weather Rev., 117, 1779–1800, 1989.

Untch, A. and Hortal, M.: A finite-element scheme for the vertical discretization of the semi-Lagrangian version of the ECMWF forecast model, Q. J. Roy. Meteor. Soc., 130, 1505–1530, doi:10.1256/qj.03.173, 2006.

Wennberg, P. O., Roehl, C., Wunch, D., Toon, G. C., Blavier, J.-F., Washenfelder, R., Keppel-Aleks, G., Allen, N., and Ayers, J.: TCCON data from Park Falls (US), Release GGG2014R0, TCCON data archive, hosted by CDIAC, doi:10.14291/tccon.ggg2014.parkfalls01.R0/1149161, 2014.

Wennberg, P. O., Wunch, D., Roehl, C., Blavier, J.-F., Toon, G. C., Allen, N., Dowell, P., Teske, K., Martin, C., and Martin, J.: TCCON data from Lamont (US), Release GGG2014R0, TCCON data archive, hosted by CDIAC, doi:10.14291/tccon.ggg2014.lamont01.R0/1149159, 2014.

Wunch, D., Toon, G. C., Blavier, J.-F. L., Washenfelder, R. A., Notholt, J., Connor, B., Griffith, D. W. T., Sherlock, V., and Wennberg, P. O.: The total carbon column observing network, Phil. T. Roy. Soc. A, 369, 2087–2112, doi:10.1098/rsta.2010.0240, 2011.

Wunch, D., Toon, G. C., Sherlock, V., Deutscher, N. M., Liu, C., Feist, D. G., and Wennberg, P. O.: The Total Carbon Column Observing Network's GGG2014 Data Version. Carbon Dioxide Information Analysis Center, Oak Ridge National Laboratory, Oak Ridge, Tennessee, USA, doi:10.14291/tccon.ggg2014.documentation.R0/1221662, 2015.